Journal of Molecular Modeling (2018) 24: 249
https://doi.org/10.1007/s00894-018-3793-6

ORIGINAL PAPER

Characterizing the sensitivity of bonds to the curvature of carbon nanotubes

Jyotirmoy Deb[1] · Debolina Paul[1] · Utpal Sarkar[1] · Paul W. Ayers[2]

Received: 19 June 2018 / Accepted: 12 August 2018 / Published online: 21 August 2018

Abstract

The way the bonding and reactivity of armchair carbon nanotubes depends on the curvature of the nanotube has been investigated using density functional theory. To understand the nature of the interaction between atoms in the nanotube, the Wiberg bond index, natural bond order analysis, and topological electron density analysis have been performed. All these tools confirm that the bonds in the hydrogen-capped carbon nanotubes considered here are primarily covalent. As the diameter of the nanotube decreases and its curvature increases, the covalency (bond order) decreases, a conclusion that is supported by the increase of the bond lengths and also the decrease of the electron density and the energy density along the bond paths as the curvature increases. To shed light on the orbital contribution in bond formation and the most effective interaction between donor bonding orbital and acceptor antibonding orbital, analysis of natural bond orbitals is carried out. We have observed that the higher the nanotube diameter is, the higher the energy gap.

Keywords Density functional theory · Curved surface · Bonding analysis · Electron density analysis · Natural bond orbital analysis · Chemical reactivity

Introduction

Besides their fundamental interest, carbon nanotubes (CNT) [1] are potentially useful for modern technologies like chemical sensors, field-effect transistors, and energy conversion/storage devices [2–5]. For many of these applications, it is essential that homogenous CNTs, with a narrow range of chiralities and sizes, are available. Of special relevance to this paper, the curvature of a CNT has significant effect on its properties. For instance, double layer capacitance increases with decreasing radius of the CNT [6], affecting the total capacitance of the system. The electronic properties, energetics [7], adsorption, and catalytic activity of CNTs also varies with their chiralities and diameter [8]. Depending on the chiralities of the carbon nanotube, nearly two-thirds of them exhibit semiconducting characteristics, while the other third have metallic character. Single-walled carbon nanotubes (SWCNTs) with metals put inside them are used in designing magnetic data storage devices, nanoscale switches, carbon nanotube field effect transistors (CNTFETs), p-n junction diodes among other nanoelectronic devices [9–11]. Nanotube chirality is responsible for defining the diameter, curvature, structural, and electronic properties [12–15]. The possibility of designing and manipulating its properties by controlling the shape, size, and constituent particles make carbon nanotubes one of the most versatile materials. They have attracted great interest because of their unique physical (elasticity, stiffness, and deformation) [16], chemical properties [17–19], and extraordinary electronic properties [20]; hence they are believed to be of great potential for next generation nanoscale electronic devices [9]. Electrons can be conducted in the nanotubes without any scattering, owing to its 1-D nature [21]. This absence of scattering is known as ballistic transport and it permits the

This paper belongs to Topical Collection International Conference on Systems and Processes in Physics, Chemistry and Biology (ICSPPCB-2018) in honor of Professor Pratim K. Chattaraj on his sixtieth birthday

Electronic supplementary material The online version of this article (https://doi.org/10.1007/s00894-018-3793-6) contains supplementary material, which is available to authorized users.

✉ Utpal Sarkar
utpalchemiitkgp@yahoo.com

✉ Paul W. Ayers
ayers@mcmaster.ca

[1] Department of Physics, Assam University, Silchar 788011, India

[2] Department of Chemistry and Chemical Biology, McMaster University, Hamilton, Ontario L8S 4M1, Canada

nanotube to conduct electrons without dissipating heat. The breadth and importance of potential applications make CNT a very active area of research, with many new challenges and opportunities for studying the chemistry of these systems. In order to control the electronic properties of CNTs and the functioning CNT-based devices, researchers have tried to characterize and control the chirality and size of the CNT.

The chirality of a CNT is uniquely characterized by a pair of nonnegative integers, (n,m), which describe how one "rolls up" a graphene sheet to form the seamless cylindrical surface of an infinite-length CNT. CNTs can be considered hollow conjugated polyaromatic macromolecules essentially with an inert interior and a reactive exterior that is sensitive to the way the parameters (n,m) describe how the graphene sheet is rolled up. Nanotubes can be classified as armchair (n = m), zigzag (n ≠ m), and chiral (m = 0). Among these, armchair (n,n) SWCNT are the most thermodynamically stable [22]. The electronic structure of finite-length short armchair nanotubes [23, 24] computed using ab initio and semiempirical quantum computational methods has been reported, and it is found that energy gap is oscillatory in nature with respect to the tube length. Further, the highest occupied molecular orbital (HOMO), the lowest unoccupied molecular orbital (LUMO), and the band-gap oscillate with respect to tubular diameter and length [25]. Scanning tunneling microscope experiments prove that armchair carbon nanotubes are metallic [17, 18]. Confinement of electrons along the tube axis affects the electronic properties, opening up an appreciable band gap in very short nanotubes. Previously, it has been reported that electronic properties like the energy gap and chemical reactivity parameters of (n,n) CNT ($n = 3–6$) are sensitive to the varying length and diameter of CNT [29] and that these parameters can be systematically tuned by adjusting the length and diameter of the tube. However, no computational studies of chemical reactivity descriptors have been reported for CNT with large diameters.

Since nanotube chirality/diameter plays an important role in their widespread applications in the field of nanoelectronics, understanding of the effect of chirality/diameter on the chemical structure and bonding properties of CNTs is critical. The bonding nature exhibited by transition metals (TM) doped fullerene [26] has predicted that TM-C bonds in these systems show partial covalent character and that the covalent character increases slightly as we move toward higher atomic number within the 3d-block. Studies of the confinement of noble gases within BN-doped carbon nanotubes show that they also exhibit pure or partial covalent character [27]. The bonding nature of C–C bond and C–M bond (M = metal) at planar surface (e.g., graphene) reflects that in the limit of infinite CNT radius, these interactions are covalent [28]. To the best of our knowledge, however, no investigation of the bonding character at the curved surface of CNTs has been reported. This is the topic of the current study. Specifically, we considered a number of armchair nanotubes with variable curvature. The highest curvature system we considered is the (5,5) CNT, whereas the lowest curvature nanotube system is the (20,20) CNT. We also considered a planar graphene ribbon (GR) that is not curved at all and can represent an ideal nanotube with infinite diameter and zero curvature. To characterize the bonding character, we used electron density analysis (EDA), the Wiberg bond index (WBI), natural population analysis (NPA), and natural bond orbital analysis (NBO).

Computational details

All quantum chemical calculations were performed using Kohn-Sham density functional theory as implemented in Gaussian 09 [30]. All the structures are fully optimized without symmetry constraints. The frequency calculation shows that these structures have no saddle point. We used Becke–Lee–Yang–Parr (BLYP) semi local functional [31, 32], Becke's three parameters Lee-Yang-Parr hybrid functional (B3LYP) [31, 32], and meta exchange-correlation hybrid functional (M06-2X) [33] along with 6-31G(d) basis set. In order to understand the nature of chemical bonding, the electron density analysis (EDA) [34] of the electron density and the local energy at bond critical points developed by Bader in the context of the quantum theory of atoms in molecules is employed. We performed EDA using the Multiwfn software [35].

The ionization potential (I) and electron affinity (A) can be approximated using Koopmans' theorem [36].

$$I = -E_{HOMO} \tag{1}$$

$$A = -E_{LUMO} \tag{2}$$

The global reactivity parameters [37], such as electronegativity (χ) [38–40], chemical potential (μ), chemical hardness (η) [41], and electrophilicity index (ω) [42, 43], are then calculated using the given relations:

$$\mu = -\chi = -\frac{I + A}{2} \tag{3}$$

$$\eta = I - A \tag{4}$$

$$\omega = \frac{\mu^2}{2\eta} \tag{5}$$

where χ is the electronegativity of the system.

Results and discussion

A detailed investigation was done to observe the structural properties, bonding nature, and chemical reactivity parameters

at the curved surface of a CNT. To see how the bonding and reactivity of the CNT changes, the nanotube diameter is increased (~7.5–27.5 Å), keeping its length fixed (~8 Å), starting from the (5,5) armchair CNT and concluding with our "largest" CNT, a graphene ribbon with infinite diameter and zero curvature. To avoid dangling bonds, surface atoms are terminated by H atoms. Optimized geometries of some representative structures are shown in Fig. 1. The geometries of the remaining structures are provided in Fig. S1 and coordinates of all the structures are given in Table S1 of the supporting information. Our study mainly concentrated on the bonds perpendicular to tube axis (C3–C11, C5–C13, C7–C15) and bonds parallel to the tube axis (H1–C2, C2–C3, C3–C4, C4–C5). There are some other bonds along the tube axis which have been ignored as the structure is symmetric about the center of the tube.

Structural properties

We start by discussing how the bond lengths and angles change as the CNT diameter increases. For the sake of simplicity, the H1–C2 bond, one parallel (C2–C3) bond and one perpendicular (C7–C15) bond with respect to the tube axis are used as probes of changes in the bond lengths with increasing tube diameter. Figure 2a clearly shows that all three bond lengths decrease monotonically with an increase in diameter, as might be expected based on the decreasing ring-strain as the CNT diameter increases. Though the change in bond lengths are not large, they give a hint about the bonding in these CNTs. Specifically, as the diameter increases, the strain produced due to the curvature between any two atoms decreases appreciably by shortening their bond distances and heading toward the flat unstrained GR, as can be observed from Fig. 2a. The change in functional (B3LYP to M06-2X) does not induce any significant change in bond lengths. However, a very small change (~1%) in bond lengths was observed for the BLYP functional compared to B3LYP and M06-2X functional (Table S2 of the supporting information). It is further found from Fig. 2b, that there is also a noticeable change, taking place in dihedral angle, C6–C5–C13–C12 of these systems and its variation is clear from small diameter (5,5) CNT (163.108^0 in the case of BLYP, 163.209^0 using B3LYP, and 163.283^0 for M06-2X functional) to planar GR (180.000^0) with decreasing curvature.

Bonding analysis

To gain further insight into the nature of bonding, we performed natural population analysis (NPA) [44] and Wiberg bond index (WBI) [45] on representative bonds in the CNTs. The WBI values and NPA charges are tabulated in Table S3 of the supporting information. The WBI values of a particular bond indicate the extent of covalent character. For all these considered systems, WBI values of parallel and perpendicular bonds with respect to tube axis show that all these bonds are nearly covalent in nature [46]. The change in WBI values for H1–C2, C3–C4, and C3–C11 bonds is not very large. However, for the C7–C15 bond the WBI decreases a bit more as the curvature increases. The magnitude of WBI also gives an indication about the bond order. If the magnitude of WBI is near one than it corresponds to a single bond and if the value is higher than one, then it is generally referred to as a double bond. The calculated WBI values reflect that H1–C2 is a single bond and the other three bonds (C3–C4, C3–C11, and C7–C15) have partial-double bond character, with the C7–C15 bond having the strongest double-bond character. The NPA charges on different atoms does not change significantly. However, for the C7 and C15 atoms, the charge on these atoms decreases with increase of curvature and thus charge density decreases along the C7–C15 fragment, which ensures the fall of covalent type interaction in this fragment.

Electron density analysis

To provide a clearer picture about the nature of the bonding in CNTs, electron density analysis (EDA) were performed [47, 48]. EDA is an especially useful technique for investigating the electronic properties of a molecular system, and especially for visualizing chemical reactions and the nature of interatomic interactions. In EDA, with the help of gradient vector field [49], the topological analysis of charge density was performed. The ridgeline of maximum charge density between two atoms is called the bond path and represents the atomic interaction line [50]. The point along this line where $\nabla\rho$ (r_c) is zero is called the bond critical point (BCP). In order to determine the strength of the interaction between two atoms, quantities such as the electron density ρ (r_c), the Laplacian of electron density $\nabla^2\rho$ (r_c), and the local electron energy density H (r_c) (which consists of two parts: local kinetic energy density G (r_c) and local potential energy density V (r_c)) can be calculated at the BCP. Though interactions in molecules are electrostatic in nature, based on the magnitudes of their topological descriptors one can classify the types of interaction. There are two types of interaction: open-shell and closed-shell interaction. The open-shell interaction results in strong covalent bonds, whereas typically weaker interactions are observed for closed-shell interactions. The energy terms of the charge density are related to its Laplacian at the BCP and are computed using the relations:

$$\frac{1}{4\nabla^2\rho(r_c)} = 2\mathrm{G}(r_c) + V(r_c) \tag{6}$$

and

$$H(r_c) = \mathrm{G}(r_c) + V(r_c) \tag{7}$$

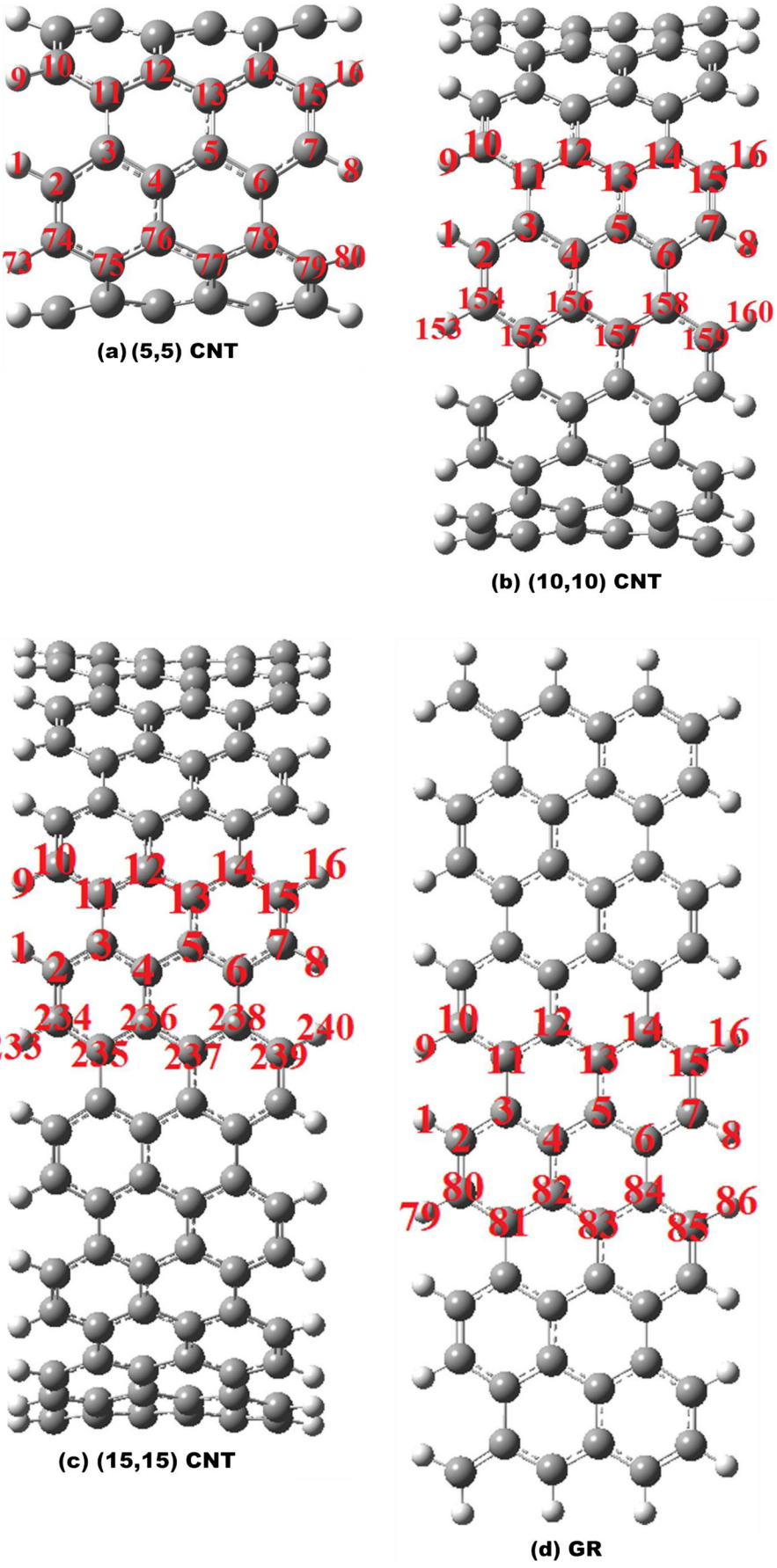

Fig. 1 Optimized geometries of (**a**) (5,5); (**b**) (10,10); (**c**) (15,15) CNT, and (**d**) GR

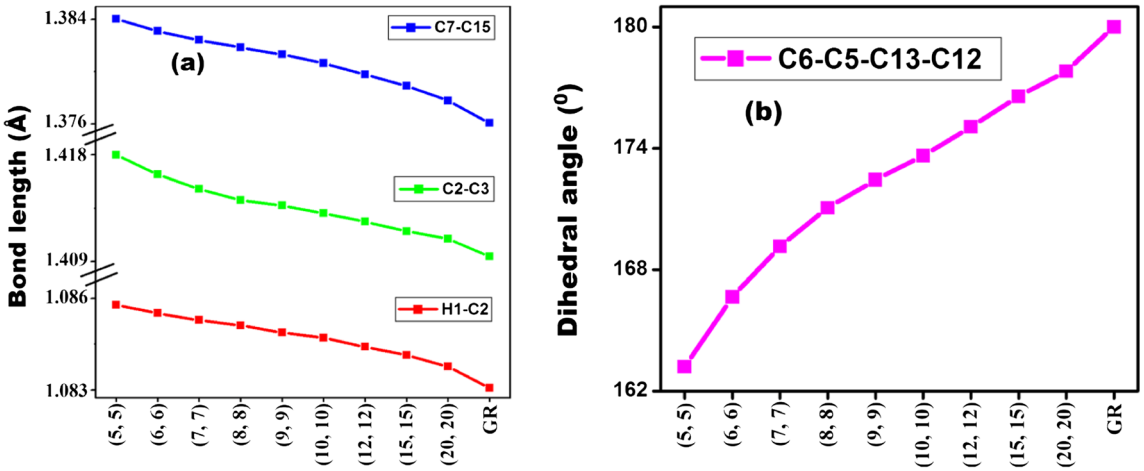

Fig. 2 Variation in (**a**) bond length; (**b**) dihedral angle; of (n,n) CNT (n = 5–10, 12, 15, 20) and GR at B3LYP/6-31G(d) level

If $\nabla^2 \rho$ (r_c) and H (r_c) are both less than zero, then the interaction is termed as an open-shell interaction, and in that case electron density is concentrated along the bond path, resulting in a covalent bond between the participating atoms. However, for a closed-shell interaction, $\nabla^2\rho$ (r_c) and H (r_c) are both greater than zero which indicates that the nature of interaction may be ionic or van der Waals type. Partial covalent character is often attributed to bonds with $\nabla^2\rho$ (r_c) greater than zero and H (r_c) less than zero.

Here we focus on the difference between the bonding nature at the curved surface and that of the planar sheet. The topological charge density analysis of CNT and GR are tabulated in Table S4 and Table S5 of the supporting information and the corresponding graphical representation of $\nabla^2\rho$ (r_c) is shown in Fig. 3. For all these systems, the magnitude of both $\nabla^2\rho$ (r_c) and H (r_c) are negative at BCPs for all the bonds we considered, which confirms that these bonds are of purely covalent character (open-shell interaction); this reinforces the interpretation from the WBI calculation. Interestingly, the degree of covalent character varies from bond to bond in different systems. For a particular structure, the degree of covalency is highest for the H1–C2 bond, whereas the C3–C11 bond exhibits the least covalent nature. Among the considered bonds, the variation is significant for perpendicular bonds compared to parallel bonds. In the case of H1–C2 and C2–C3 bonds, the degree of covalent character is highest for the planar GR system and it decreases to a slight extent as we increase the curvature of the system, but for other bonds along the axis, variation is not very remarkable. However, a significant change in the extent of covalent character was observed for C7–C15 and C3–C11 bonds. The effect of curvature on these two bonds results in strong decrement in covalent nature, as measured by a decrease in density at the BCP, along with a decrease in the magnitude of the (negative) Laplacian and energy density at the BCP. In order to check the effect of length on bonding character of GR, two longer systems were considered, one 35 Å in length and the other 48 Å in length apart from the previously considered GR of length 22 Å. The increase in length of GR does not affect much about the extent of covalent character of the selected bonds, but a slight increase in covalent character is noted for the C3–C11 perpendicular bond.

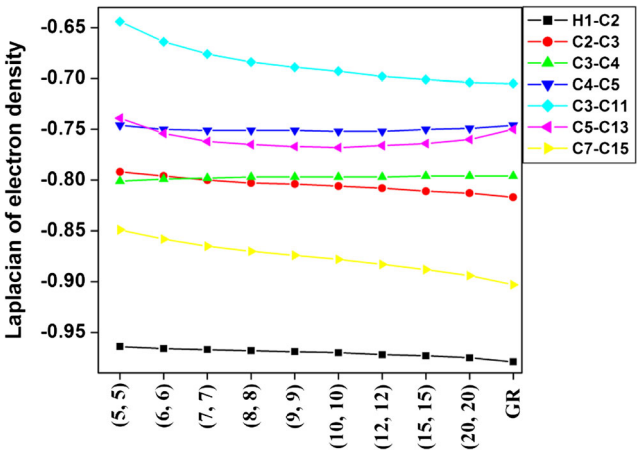

Fig. 3 Variation of Laplacian of electron density of different bonds of (n,n) CNT (n = 5–10, 12, 15, 20) and GR at B3LYP/6-31G(d) level

The contour plot of $\nabla^2\rho$ (r_c) is provided in Fig. 4 in which the green-colored portion represents regions where the charge density is depleted (i.e., $\nabla^2 \rho$ (r_c) >0), while the blue-colored portion represents regions where the charge density region accumulates (i.e., $\nabla^2 \rho$ (r_c) <0). The associated bond paths and interatomic surfaces are also plotted.

Natural bond orbital (NBO) analysis

NBO analysis [51] is a method to determine the most important Lewis structure (s) for describing a molecule. It gives useful information for studying intra- and inter-molecular interactions between filled and virtual orbitals of various bonds. Bonding concepts like the type of bond orbitals, their

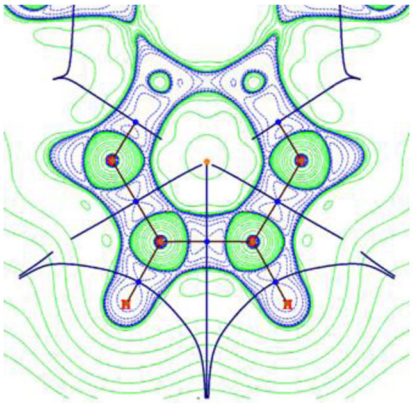

(5,5) CNT

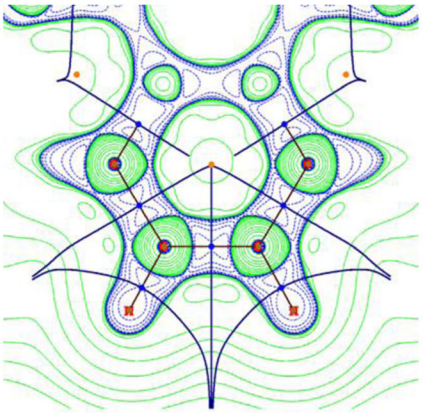

(6,6) CNT

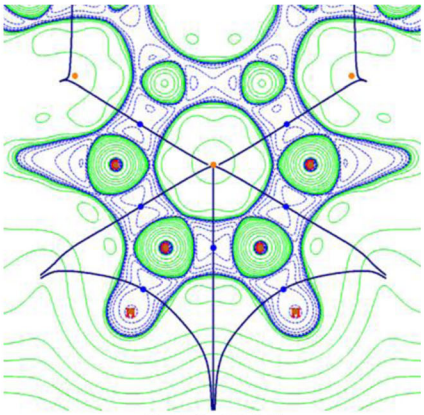

(7,7) CNT

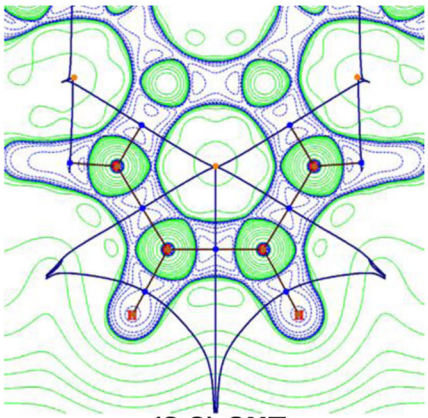

(8,8) CNT

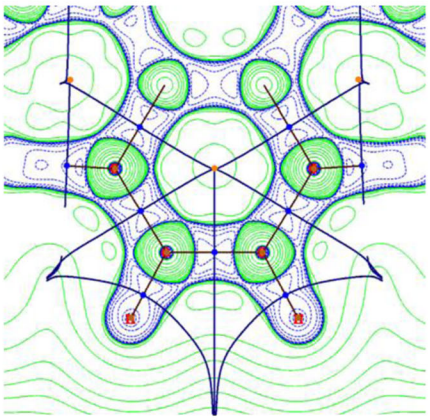

(9,9) CNT

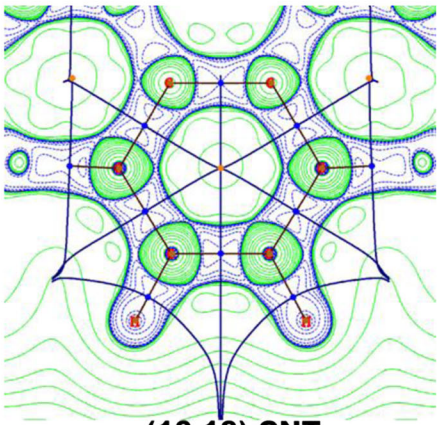

(10,10) CNT

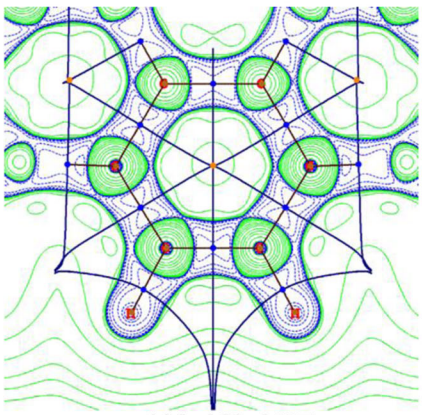

(12,12) CNT

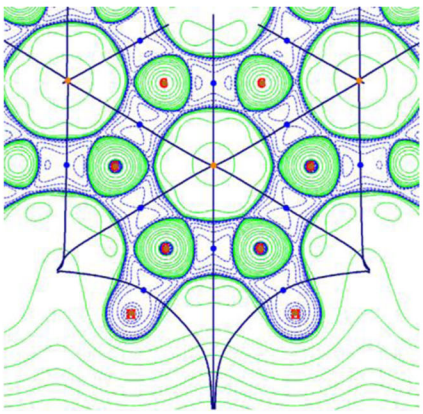

(15,15) CNT

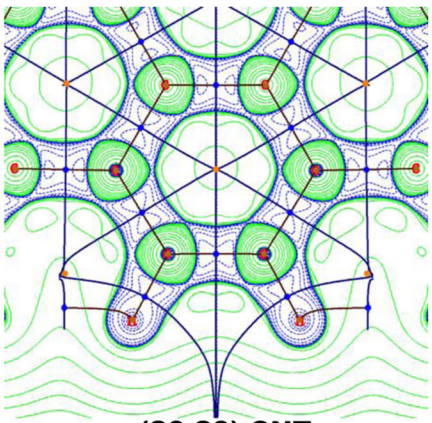

(20,20) CNT

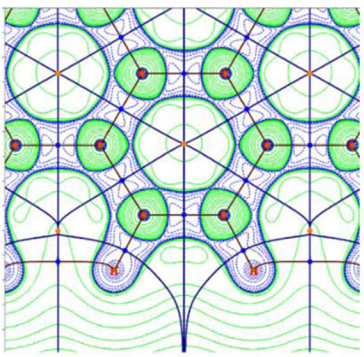

GR

◀ **Fig. 4** Contour plots of Laplacian of electron density of (n,n) CNT (n = 5–10, 12, 15, 20) and GR at a particular plane obtained using B3LYP/6-31G(d) level. The green region depicts the area having $\nabla^2 \rho\,(r_c) > 0$, and the blue region depicts the area having $\nabla^2 \rho\,(r_c) < 0$

occupancies, the accumulation of electron density in the atoms participating in the bonding, the atomic hybrid orbitals that contribute to each natural bond orbital (NBO) and their relative contribution, and the amount of s and p character present in each atomic hybrid orbital (e.g., sp^x) are presented in Table S6 and Table S7 of the supporting information. For the (5,5) CNT, the H1–C2 bonding orbital, with 1.9777 electrons has 38.32% H character with s hybrid and the C atom contributes 61.68% of the bonding orbital in the $sp^{2.43}$ hybrid. Unsurprisingly, the orbital contribution by the H atom is fully s in character, whereas the carbon orbital has predominantly p character (70.81%), consistent with a near sp^3 character of the carbon atoms at the edge of the CNT. The magnitudes of polarization coefficients are 0.6190 and 0.7854, and their sizes signify the importance of the two hybrids in the bond formation. The contribution of the C atom to the NBO is higher, so the bond is polarized somewhat toward the carbon atom. This may be due to an electronegativity difference between two participating elements. For C7–C15, there are two bonding orbitals: one associated with the single bond and other linked to the double bond. By symmetry, both orbitals have equal electron density concentration at C7 and C15 atoms. The bonding orbitals have 64.20 and 99.52% p character for both the C atoms related to the single and double bond respectively. The increase in diameter introduces slight changes in various parameters of NBOs. Specially, for C7=C15 bonding orbital, p character increases with an increase in diameter, and in the case of GR it has 99.95% p character.

The second order perturbation theory of the Fock matrix calculation was used to investigate the most effective donor-acceptor interactions in NBO analysis and measure the delocalization of the electron density or hyperconjugation. The interaction results in loss of occupancy due to concentration difference between the NBOs of the idealized Lewis structure and empty non-Lewis orbitals. The stabilization energy ($\mathbf{E^{(2)}}$) corresponding to delocalization of $i \rightarrow j$ for each interaction is given by:

$$E^{(2)} = \Delta E_{ij} = q_i \frac{F^2(i,j)}{E_j - E_i} \tag{8}$$

where q_i is donor orbital occupancy, E_i and E_j are energies of diagonal elements, and $F(i,j)$ is off diagonal Fock matrix element. The most important acceptor–donor second order perturbation energies (in kcal mol^{-1}) of some selected bonds are listed in Table 1. The highest value of stabilization energy indicates strong interaction between electron donors and acceptors (i.e., the extent of conjugation is high). For the studied systems, the most significant interaction is observed for bonding orbital π (C7–C15) – antibonding orbital π* (C5–C6 or C13–C14) as the stabilization energy is highest for this interaction. The magnitude of $\mathbf{E^{(2)}}$ increases sharply for all selected interactions as we move from smaller diameter to larger diameter. However, the increment of $\mathbf{E^{(2)}}$ is significant for π (C7–C15) – π* (C5–C6 or C13–C14) interaction. The increase in stabilization energy results from the intermolecular charge transfer between donor orbital and acceptor orbital. This interaction may arise due to enhanced electron density in the antibonding orbital, weakening the corresponding bond. Among all considered interactions of different systems, the π (C2–C3) to π* (C5–C6 or C13–C14) interaction is most prominent as it possesses the highest stabilization energy.

Chemical reactivity parameters

The energy gap between the frontier molecular orbitals (highest occupied molecular orbital, HOMO and lowest unoccupied molecular orbital, LUMO) is an important factor for stability and chemical reactivity analysis. It is experimentally verified that infinite-length single-walled armchair CNTs and GR are metallic in nature [15, 52, 53], a conclusion supported by Huckel theory [22]. In this paper, we studied relatively short CNT and GR with the ends saturated by hydrogen atoms, hence we expect appreciable nonzero band gap for these structures. The band gap in hydrogen terminated CNT and GR arises due to quantum confinement and crucial effect due to edges [54, 55]. Though GR possesses a small band gap, its magnitude decreases with increase in length of GR [54, 55]. The molecular orbital energies (E_{HOMO} and E_{LUMO}) and chemical reactivity parameters [37–43, 56], such as η, μ, and ω, are listed in Tables 2 and 3. For (20,20) CNT the energy gap is highest (Table 3), and it decreases gradually with an increase in curvature or decrease in diameter irrespective of functional used. The large energy difference between HOMO and LUMO indicates the system is reluctant to accommodate any extra electron in LUMO nor it is susceptible to losing an electron from HOMO. For (5,5) armchair CNT, the DFT calculation by Zhou et al. [57] for the three-unit cell predicted the HOMO-LUMO gap to be 1.56 eV, and this is in good agreement with our result obtained using B3LYP functional (1.554 eV) for the same type of CNT. A DFT study by Galano [29] predicted very small HOMO-LUMO gaps for three-unit cell (4,4), (5,5), and (6,6) CNTs as 0.25, 0.55, and 0.82 eV respectively calculated at the PM3 level of theory, i.e., the gap increases with increasing diameter. Our calculation shows the same trend not only for (5,5), (6,6) CNTs, but also for other CNTs. In our work the magnitude of the HOMO-LUMO gap is quite high for B3LYP and M06-2X functionals, and this difference is due to the different levels of theory used

Table 1 Second order perturbation theory analysis of Fock matrix of (n,n) CNT ($n = 5$–10, 12, 15, 20) and GR associated with some selected donor-acceptor interactions calculated using B3LYP and M06-2X functional

System	Donor NBO (i)	Acceptor NBO (j)	$E^{(2)}$ (kcal mol^{-1})		E (j)-E (i) (au)	
			B3LYP	M06-2X	B3LYP	M06-2X
(5,5) CNT	BD(1) H1–C2	BD*(1) C74–C75	4.30	4.55	1.14	1.21
	BD(1) C2–C3	BD*(1) C3–C4	4.21	4.24	1.31	1.39
	BD(2) C7–C15	BD*(2) C5–C6	16.69	20.82	0.33	0.38
	BD(2) C7–C15	BD*(2) C13–C14	16.68	20.81	0.33	0.38
(6,6) CNT	BD(1) H1–C2	BD*(1) C90–C91	4.35	4.59	1.14	1.21
	BD(1) C2–C3	BD*(1) C3–C4	4.27	4.30	1.31	1.39
	BD(2) C7–C15	BD*(2) C5–C6	17.29	21.57	0.33	0.37
	BD(2) C7–C15	BD*(2) C13–C14	17.30	21.56	0.33	0.37
(7,7) CNT	BD(1) H1–C2	BD*(1) C106–C107	4.39	4.62	1.14	1.22
	BD(1) C2–C3	BD*(1) C3–C4	4.31	4.34	1.32	1.40
	BD(2) C7–C15	BD*(2) C5–C6	17.68	22.06	0.33	0.37
	BD(2) C7–C15	BD*(2) C13–C14	17.69	22.09	0.33	0.37
(8,8) CNT	BD(1) H1–C2	BD*(1) C122–C123	4.43	4.66	1.14	1.22
	BD(1) C2–C3	BD*(1) C3–C4	4.33	4.36	1.32	1.32
	BD(2) C7–C15	BD*(2) C5–C6	17.97	22.41	0.33	0.37
	BD(2) C7–C15	BD*(2) C13–C14	17.98	22.42	0.33	0.37
(9,9) CNT	BD(1) H1–C2	BD*(1) C138–C139	4.44	4.67	1.15	1.22
	BD(1) C2–C3	BD*(1) C3–C4	4.36	4.38	1.32	1.40
	BD(2) C7–C15	BD*(2) C5–C6	18.18	22.62	0.33	0.37
	BD(2) C7–C15	BD*(2) C13–C14	18.18	22.63	0.33	0.37
(10,10) CNT	BD(1) H1–C2	BD*(1) C154–C155	4.46	4.70	1.15	1.22
	BD(1) C2–C3	BD*(1) C3–C4	4.37	4.39	1.32	1.40
	BD(2) C7–C15	BD*(2) C5–C6	18.33	22.84	0.33	0.37
	BD(2) C7–C15	BD*(2) C13–C14	18.33	22.86	0.33	0.37
(12,12) CNT	BD(1) H1–C2	BD*(1) C186–C187	4.50	4.70	1.15	1.22
	BD(1) C2–C3	BD*(1) C3–C4	4.39	4.42	1.32	1.40
	BD(2) C7–C15	BD*(2) C5–C6	18.54	23.10	0.33	0.37
	BD(2) C7–C15	BD*(2) C13–C14	18.55	23.10	0.33	0.37
(15,15) CNT	BD(1) H1–C2	BD*(1) C234–C235	4.53	4.73	1.15	1.23
	BD(1) C2–C3	BD*(1) C3–C4	4.41	4.44	1.32	1.40
	BD(2) C7–C15	BD*(2) C5–C6	18.76	23.32	0.32	0.37
	BD(2) C7–C15	BD*(2) C13–C14	18.76	23.33	0.32	0.37
(20,20) CNT	BD(1) H1–C2	BD*(1) C309–310	4.56	4.77	1.15	1.23
	BD(1) C2–C3	BD*(1) C3–C4	4.41	4.44	1.32	1.40
	BD(2) C7–C15	BD*(2) C5–C6	18.94	23.52	0.32	0.37
	BD(2) C7–C15	BD*(2) C13–C14	18.94	23.51	0.32	0.37
GR	BD(1) H1–C2	BD*(1) C45–C46	4.63	4.84	1.15	1.23
	BD(1) C2–C3	BD*(1) C3–C4	4.44	4.46	1.32	1.40
	BD(2) C7–C15	BD*(2) C5–C6	19.31	23.88	0.32	0.37
	BD(2) C7–C15	BD*(2) C13–C14	19.33	23.90	0.32	1.21

BD (1/2) = single/double bonding orbital, BD* (1/2) = single/double antibonding orbital

for calculation. However, in the case of the BLYP functional, the gap is relatively small compared to the other two functionals used here. With an increase in diameter, hardness (η) of the studied systems increases, whereas electrophilicity index (ω) decreases. All functionals follow the same trend; however, magnitude of η (or **ω**) is quite high (or low) for the M06-2X functional with respect to BLYP and B3LYP functionals. Therefore, these systems obeyed two fundamental principles: maximum hardness principle (MHP) [58–60] and minimum electrophilicity principle

Table 2 The molecular orbital energies (E_{HOMO} and E_{LUMO}) of (n,n) CNT ($n = 5–10$, 12, 15, 20) and GR calculated using BLYP, B3LYP, and M06-2X functionals

Systems	E_{HOMO} (eV)			E_{LUMO} (eV)		
	BLYP	B3LYP	M06-2X	BLYP	B3LYP	M06-2X
(5,5)	−3.523	−4.164	−5.190	−2.847	−2.610	−2.073
(6,6)	−3.615	−4.249	−5.271	−2.817	−2.590	−2.067
(7,7)	−3.677	−4.307	−5.327	−2.800	−2.580	−2.065
(8,8)	−3.720	−4.350	−5.370	−2.791	−2.572	−2.061
(9,9)	−3.753	−4.382	−5.404	−2.784	−2.567	−2.057
(10,10)	−3.777	−4.405	−5.430	−2.779	−2.564	−2.057
(12,12)	−3.812	−4.441	−5.468	−2.773	−2.561	−2.055
(15,15)	−3.845	−4.475	−5.504	−2.770	−2.557	−2.054
(20,20)	−3.873	−4.506	−5.537	−2.770	−2.557	−2.056
GR	−3.384	−3.668	−4.019	−3.383	−3.517	−3.607
GR_one_half	−3.388	−3.643	−3.945	−3.387	−3.553	−3.700
GR_two	−3.390	−3.632	−3.912	−3.389	−3.568	−3.738

(MEP) [61]. Among the CNTs considered in this work, the (20,20) CNT is the most stable nanotube because it has the highest η value. We expect it to be very difficult to polarize such a system because the maximum hardness principle (MHP) is related to the minimum polarizability principle (MPP) [62]. In order to polarize such a system more energy has to be supplied for excitation, and consequently it shows low reactivity profile. Chemical potential (or electronegativity) decreases (or increases) for larger diameter CNTs implying the fact that if two CNTs with different diameters but equal length interact with each other, then the electron will always flow from the lower diameter nanotube to the higher diameter nanotube since the chemical potential of the lower diameter nanotube is higher. The theoretically calculated chemical reactivity parameters for three-unit cells of (5,5) and (6,6) CNTs are in close accordance with previous theoretical findings [29, 57].

Conclusions

A systemetic study has been performed to investigate the effect of curvature on bonding and various electronic properties of carbon nanotubes (CNT). The Wiberg bond index (WBI) reflects that all selected bonds are purely covalent in character, a result that is confirmed by the negative values of $\nabla^2\rho$ (r_c) and H (r_c) at the bond critical points (BCPs) of all the bonds we studied. The reduction (becoming more negative) of $\nabla^2\rho$ (r_c) and H (r_c) and the increase of ρ (r_c) with increasing CNT diameter confirms that as the bond strain in the CNT decreases the covalency increases. This is confirmed by the shortening of the bonds in the CNTs and a natural bond order analysis. Interestingly, perpendicular bonds show greater higher-double-bond character than the parallel bonds. This may be because the effects of truncating the CNT (the boundary effects) are least significant when one considers bonds that are

Table 3 Chemical hardness (η), chemical potential (μ), and electrophilicity index (ω) of (n,n) CNT (n = 5–10, 12, 15, 20) and GR calculated using BLYP, B3LYP, and M06-2X functionals

Systems	η (eV)			μ (eV)			ω (eV)		
	BLYP	B3LYP	M06-2X	BLYP	B3LYP	M06-2X	BLYP	B3LYP	M06-2X
(5,5)	0.676	1.554	3.117	−3.185	−3.387	−3.632	7.503	3.691	2.115
(6,6)	0.798	1.659	3.204	−3.216	−3.420	−3.669	6.480	3.525	2.101
(7,7)	0.877	1.727	3.262	−3.239	−3.444	−3.696	5.981	3.454	2.094
(8,8)	0.929	1.778	3.309	−3.256	−3.461	−3.716	5.706	3.369	2.086
(9,9)	0.969	1.815	3.347	−3.269	−3.475	−3.731	5.514	3.327	2.079
(10,10)	0.998	1.841	3.373	−3.278	−3.485	−3.744	5.383	3.299	2.077
(12,12)	1.039	1.880	3.413	−3.293	−3.501	−3.762	5.218	3.260	2.073
(15,15)	1.075	1.918	3.450	−3.308	−3.516	−3.779	5.090	3.223	2.070
(20,20)	1.103	1.949	3.481	−3.322	−3.532	−3.797	5.003	3.200	2.070
GR	0.001	0.151	0.412	−3.384	−3.593	−3.813	5725.728	42.747	17.644

perpendicular to the boundary. The bond order of the C7–C15 and C3–C11 bonds decreases noticeably with increasing curvature, which is consistent with the decreasing accumulation of electron density along the bond path (BP) for these systems. NBO analysis indicates that, for most of the systems we consider, the $\pi - \pi^*$ interaction between donor orbital C7–C15 and acceptor orbital C5–C6 or C13–C14 is significant and has a higher stabilization energy than other interactions. Among the considered nanotubes, chemical reactivity parameters indicate that hardness increases and electrophilicity decreases with the increase of tube diameter, i.e., stability of nanotubes increases with the increase of diameter or decrease of curvature of the nanotube.

Acknowledgments The authors dedicate this work to celebrate the 60th birthday of Prof. P. K. Chattaraj. JD thanks, the Department of Science and Technology, India for the INSPIRE fellowship. US and PWA thank Compute Canada for providing computational facilities for this research work. PWA thanks NSERC and the Canada Research Chairs for funding.

References

1. Iijima S (1991) Helical microtubules of graphitic carbon. Nature 354:56–58
2. Ioannatos GE, Verykios XE (2010) H2 storage on single- and multi-walled carbon nanotubes. Int J Hydrog Energy 35:622–628
3. Singh NB, Bhattacharya B, Mondal R, Sarkar U (2016) Nickel cluster functionalised carbon nanotube for CO molecule detection: a theoretical study. Mol Phys 114:671–680
4. Schnorr JM, Swager TM (2011) Emerging applications of carbon nanotubes. Chem Mater 23:646–657
5. Park RS, Hills G, Sohn J, Mitra S, Shulaker MM, Philip Wong H-S (2017) Hysteresis-free carbon nanotube field-effect transistors. ACS Nano 11:4785–4791
6. Huang J, Sumpter BG, Meunier V, Yushin G, Portet C, Gogotsi Y (2010) Curvature effects in carbon nanomaterials: Exohedral versus endohedral supercapacitors. J Mater Res 25:1525–1531
7. Akhavana M, Jalili S, Schofield J (2015) Effect of diameter and chirality on the structure and electronic properties of BC2N nanotubes. Chem Phys 455:88–93
8. Chen Y, Yin S, Li Y, Cen W, Li J, Yin H (2017) Curvature dependence of single-walled carbon nanotubes for SO2 adsorption and oxidation. Appl Surf Sci 404:364–369
9. Tans SJ, Verschueren RM, Dekker C (1998) Room-temperature transistor based on a single carbon nanotube. Nature 393:49–52
10. Che G, Lakshmi BB, Martin CR, Fisher ER (1999) Metal-nanocluster-filled carbon nanotubes: catalytic properties and possible applications in electrochemical energy storage and production. Langmuir 15:750–758
11. Sevensson K, Olin H, Olsson E (2004) Nanopipettes for Metal Transport. Phys Rev Lett 93:145901–145904
12. Mintmire JW, Dunlap BI, White CT (1992) Are fullerene tubules metallic? Phys Rev Lett 68:631–634
13. Hamada N, Sawada S, Oshiyama A (1992) New one-dimensional conductors: graphitic microtubules. Phys Rev Lett 68:1579–1581
14. Odom TW, Huang JL, Kim P, Lieber CM (1998) Atomic structure and electronic properties of single-walled carbon nanotubes. Nature 391:62–64
15. Wildöer JWG, Venema LC, Rinzler AG, Smalley RE, Dekker C (1998) Electronic structure of atomically resolved carbon nanotubes. Nature 391:59–62
16. Mickelson ET, Huffman CB, Rinzler AG, Smalley RE, Hauge RH, Margrave JL (1998) Fluorination of single-wall carbon nanotubes. Chem Phys Lett 296:188–194
17. Chen J, Hamon MA, Hui H, Chen Y, Rao AM, Eklund PC, Haddon RC (1998) Solution properties of single-walled carbon nanotubes. Science 282:95–98
18. Hamwi A, Alvergnat H, Bonnamy S, Béguin F (1997) Fluorination of carbon nanotubes. Carbon 357:723–728
19. Mawhinney DB, Naumenko V, Kuznetsova A (2000) Infrared spectral evidence for the etching of carbon nanotubes: ozone oxidation at 298 K. J Am Chem Soc 122:2383–2384
20. Colbert DT, Smalley RE (1999) Fullerene nanotubes for molecular electronics. Trends Biotechnol 17:46–50
21. Karousis N, Tagmatarchis N (2010) Current progress on the chemical modification of carbon nanotubes. Chem Rev 110:5366–5397
22. Dresselhauss MS, Dresselhauss G, Eklund PC (1996) Science of fullerenes and carbon nanotubes. Academic, New York
23. Okotrub AV, Bulusheva LG, Tomanek D (1998) X-ray spectroscopic and quantum–chemical study of carbon tubes produced in arc-discharge. Chem Phys Lett 289:341–349
24. Li J, Zhang Y, Zhang M (2002) The electronic structure and its theoretical simulation of carbon nanotube with finite length. Part II: the energy gap and its oscillation properties of short armchair nanotubes. Chem Phys Lett 364:338–344
25. Wang BC, Wang HW, Lin IC (2003) A Semiempirical study of carbon nanotubes with finite tubular length and various tubular diameters. J Chin Chem Soc 50:939–945
26. Du J, Sun X, Chen J, Jiang G (2014) Understanding the stability, bonding nature and chemical reactivity of 3d-substituted heterofullerenes C_{58}TM (TM = Sc–Zn) from DFT studies. RSC Adv 4:44786–44794
27. Chakraborty D, Chattaraj PK (2015) Confinement induced binding in noble gas atoms within a BN-doped carbon nanotube. Chem Phys Lett 621:29–34
28. Wang H, Feng Q, Cheng Y, Yao Y, Wang Q, Li K, Schwingenschlögl U, Zhang XX, Yang W (2013) Atomic bonding between metal and graphene. J Phys Chem C 117:4632–4638
29. Galano A (2006) On the influence of diameter and length on the properties of armchair single-walled carbon nanotubes: a theoretical chemistry approach. Chem Phys 327:159–170
30. Frisch MJ et al (2016) Gaussian 09, revision D.01. Gaussian Inc., Wallingford
31. Becke AD (1993) Density-functional thermochemistry. III. The role of exact exchange. J Chem Phys 98:5648–5652
32. Lee C, Yang W, Parr RG (1988) Development of the Colle-Salvetti correlation-energy formula into a functional of the electron density. Phys Rev B 37:785–789
33. Zhao Y, Truhlar DG (2006) The M06 suite of density functionals for main group thermochemistry, thermochemical kinetics, noncovalent interactions, excited states, and transition elements: two new functionals and systematic testing of four M06-class functionals and 12 other functionals. Theor Chem Accounts 120:215–241
34. Bader RFW (1990) Atoms in molecules: a quantum theory. Clarendon, Oxford
35. Lu T, Chen F (2012) Multiwfn: a multifunctional wavefunction analyzer. J Comput Chem 33:580–592
36. Koopmans TA (1933) Über die Zuordnung von Wellenfunktionen und Eigenwerten zu den Einzelnen Elektronen Eines Atoms. Physica 1:104–113
37. Chattaraj PK (2009) Chemical reactivity theory: a density functional view. Taylor and Francis, Boca Raton

38. Parr RG, Donnelly RA, Levy M, Palke WE (1978) Electronegativity: the density functional viewpoint. J Chem Phys 68:3801–3807
39. Parr RG (2000) Density-functional theory and chemistry. Condens Matter Theor 15:297–302
40. Parr RG, Pearson RG (1983) Absolute hardness: companion parameter to absolute electronegativity. J Am Chem Soc 105:7512–7516
41. Ayers PW (2007) The physical basis of the hard/soft acid/base principle. Faraday Discuss 135:161–190
42. Parr RG, Szentpály LV, Liu S (1999) Electrophilicity index. J Am Chem Soc 121:1922–1924
43. Chattaraj PK, Sarkar U, Roy DR (2006) Electrophilicity index. Chem Rev 106:2065–2091
44. Reed AE, Weinstock RB, Weinhold F (1985) Natural population analysis. J Chem Phys 83:735–746
45. Wiberg KB (1968) Application of the pople-santry-segal CNDO method to the cyclopropylcarbinyl and cyclobutyl cation and to bicyclobutane. Tetrahedron 24:1083–1096
46. Jana G, Saha R, Pan S, Kumar A, Merino G, Chattaraj PK (2016) Noble gas binding ability of metal-bipyridine monocationic complexes (metal = Cu, Ag, Au): a computational study. ChemistrySelect 18:5842–5849
47. Jana G, Pan S, Chattaraj PK (2017) Binding of small gas molecules by metal–bipyridyl monocationic complexes (metal = Cu, Ag, Au) and possible bond activations therein. J Phys Chem A 121:3803–3817
48. Ghara M, Pan S, Deb J, Kumar A, Sarkar U, Chattaraj PK (2016) A computational study on structure, stability and bonding in noble gas bound metal nitrates, sulfates and carbonates (metal=Cu, Ag, Au). J Chem Sci 128:1537–1548
49. Bader RFW, Beddall PM (1972) Virial field relationship for molecular charge distributions and the spatial partitioning of molecular properties. J Chem Phys 56:3320–3329
50. Runtz GR, Bader RFW, Messer RR (1977) Definition of bond paths and bond directions in terms of the molecular charge distribution. Can J Chem 55:3040–3045
51. Reed AE, Curtiss LA, Weinhold F (1988) Intermolecular interactions from a natural bond orbital, donor-acceptor viewpoint. Chem Rev 88:899–926
52. Ajayan PM (1999) Nanotubes from carbon. Chem Rev 99:1787–1799
53. Nakada K, Fujita M, Dresselhaus G, Dresselhaus MS (1996) Edge state in graphene ribbons: nanometer size effect and edge shape dependence. Phys Rev B 54:17954–17961
54. Son Y-W, Cohen ML, Louie SG (2006) Energy gaps in graphene nanoribbons. Phys Rev Lett 97:216803–216804
55. Mandal B, Sarkar S, Pramanik A, Sarkar P (2012) Electronic structure and transport properties of sulfur-passivated graphene nanoribbons. J Appl Phys 112:113710–113716
56. Chattaraj PK, Maiti B, Sarkar U (2003) Philicity: a unified treatment of chemical reactivity and selectivity. J Phys Chem A 107:4973–4975
57. Zhou Z, Steigerwald M, Hybertsen M, Brus L, Friesner RA (2004) Electronic structure of tubular aromatic molecules derived from the metallic (5,5) armchair single wall carbon nanotube. J Am Chem Soc 126:3597–3607
58. Pearson RG (1987) Recent advances in the concept of hard and soft acids and bases. J Chem Educ 64:561–567
59. Parr RG, Chattaraj PK (1991) Principle of maximum hardness. J Am Chem Soc 113:1854–1855
60. Ayers PW, Parr RG (2000) Variational principles for describing chemical reactions: the Fukui function and chemical hardness revisited. J Am Chem Soc 122:2010–2018
61. Chamorro E, Chattaraj PK, Fuentealba P (2003) Variation of the electrophilicity index along the reaction path. J Phys Chem A 107:7068–7072
62. Chattaraj PK, Sarkar U, Roy DR (2007) Electronic structure principles and aromaticity. J Chem Educ 84:354–357